Available online at www.sciencedirect.com
ScienceDirect
Journal of Power Sources 171 (2007) 763–777
JOURNAL OF POWER SOURCES
www.elsevier.com/locate/jpowsour

A single-phase model for liquid-feed DMFCs with non-Tafel kinetics

Marcos Vera *

Área de Mecánica de Fluidos, Universidad Carlos III de Madrid, Avda. de la Universidad 30, 28911 Leganés, Spain

Received 1 December 2006; received in revised form 3 May 2007; accepted 26 May 2007
Available online 6 June 2007

Abstract

An isothermal single-phase 3D/1D model for liquid-feed direct methanol fuel cells (DMFC) is presented. Three-dimensional (3D) mass, momentum and species transport in the anode channels and gas diffusion layer is modeled using a commercial, finite-volume based, computational fluid dynamics (CFD) software complemented with user supplied subroutines. The 3D model is locally coupled to a one-dimensional (1D) model accounting for the electrochemical reactions in both the anode and the cathode, which provides a physically sound boundary condition for the velocity and methanol concentration fields at the anode gas diffusion layer/catalyst interface. The 1D model – comprising the membrane–electrode assembly, cathode gas diffusion layer, and cathode channel – assumes non-Tafel kinetics to describe the complex kinetics of the multi-step methanol oxidation reaction at the anode, and accounts for the mixed potential associated with methanol crossover, induced both by diffusion and electro-osmotic drag. Polarization curves computed for various methanol feed concentrations, temperatures, and methanol feed velocities show good agreement with recent experimental results. The spatial distribution of methanol in the anode channels, together with the distributions of current density, methanol crossover and fuel utilization at the anode catalyst layer, are also presented for different opperating conditions.

Keywords: Fuel cell; Methanol; Non-Tafel kinetics; Crossover; CFD; Modeling

1. Introduction

Fuel cells are electrochemical devices that convert the chemical energy of an energy carrier – typically hydrogen – and an oxidizer – typically the oxygen of the air – directly into electricity and heat. In contrast to the most common proton exchange membrane fuel cells (PEMFCs), operating with hydrogen, liquid-feed direct methanol fuel cells (DMFCs) use methanol as energy carrier, which makes them good candidates as small autonomous power sources. In fact, due to the high energy density of methanol, up to 100 times higher than state-of-the-art lithium-ion batteries, DMFCs are regarded as a potential substitute to conventional power generating equipment for portable electronic devices.

Nevertheless, DMFCs suffer from two fundamental problems: (i) the slow kinetics of the methanol electro-oxidation reaction and (ii) the ability of methanol to permeate through the polymer membrane crossing from anode to cathode (methanol crossover). In addition, there are several system design issues, such as water/gas/heat management or flow-field design and optimization, that still need a better understanding. The above difficulties, together with additional technological problems concerning auxiliar devices, such as pumps, fuel storage tanks, power conditioning devices, etc. have motivated a large body of work in the field during the last decade, combining mathematical and numerical modeling with detailed experimental research. Particularly, the progress in DMFC modeling has been significant.

Several mathematical models for DMFCs can be found in the literature, including early one-dimensional models [1–9] and more recent two- and three-dimensional models [10–14]. Of particular relevance is the development of models which account for multiphase flow and transport phenomena, such as the seminal work of Wang and Wang [15] or other similar models [16,17]. However, single-phase models such as the one presented here have also contributed to the understanding of the complex phenomena involved in DMFCs (see, e.g., Refs. [3–5,8,12–14,18–20]). An extensive review of this work can be found elsewhere [21,22] and will not be repeated here for brevity.

* Corresponding author. Tel.: +34 91 624 9987; fax: +34 91 624 9430.
E-mail address: marcos.vera@uc3m.es.

0378-7753/$ – see front matter © 2007 Published by Elsevier B.V.
doi:10.1016/j.jpowsour.2007.05.098

Nomenclature

a	effective catalyst surface area per unit volume (m^{-1})
A	surface area (m^2)
C	molar concentration ($mol\,m^{-3}$)
D_i	mass diffusivity of species i ($m^2\,s^{-1}$)
E	electromotive force (V)
F	Faraday's constant ($C\,mol^{-1}$)
h	convective mass transfer coefficient ($m\,s^{-1}$)
i	current density ($A\,m^{-2}$)
I	current (A)
K	permeability (m^2)
L	channel length (m)
n_d^i	electro-osmotic drag coefficient of species i
N	molar flux ($mol\,m^{-2}\,s^{-1}$)
p	pressure (Pa)
R	universal gas constant ($J\,mol^{-1}\,K^{-1}$)
$\mathbf{S}_u$	source term appearing in the momentum equation
T	temperature (K)
$\mathbf{u}$	(superficial) velocity vector ($m\,s^{-1}$)
V	actual cell voltage (V)
W	molecular weight ($kg\,mol^{-1}$)
x	coordinate along the channel (m)
y	coordinate across the channel height (m)
z	coordinate across the channel width (m)

Greek letters

α	overall mass transfer coefficient ($m\,s^{-1}$)
δ	thickness (m)
ϵ	porosity
η	overpotential (V)
κ	experimental constant
λ	experimental constant ($mol\,m^{-3}$)
μ	dynamic viscosity ($kg\,m^{-1}\,s^{-1}$)
ρ	density ($kg\,m^{-3}$)
σ	electric conductivity ($S\,m^{-1}$)

Subscripts

a	anode
ac	anode chanel
acl	anode catalyst layer
agdl	anode gas diffusion layer
amb	ambient
avg	average value
c	cathode
cc	cathode chanel
ccl	cathode catalyst layer
cgdl	cathode gas diffusion layer
CO_2	carbon dioxide
cross	crossover
d	drag
e	electronic
i	species i
in	channel inlet
m	methanol
mem	membrane
O_2	oxygen
p	parasitic
ref	reference value
w	water

Superscripts

0	standard conditions
eff	effective value
m	methanol
O_2	oxygen
w	water

Typically, the anode of a liquid-feed DMFC is supplied with a diluted methanol aqueous solutions, while the cathode is feed with an oxidizer stream (air or pure oxygen) which can be either forced by an external blower or driven by natural convection. Due to the combined effect of both convection and diffusion the methanol and the oxygen reach the anode and cathode catalyst layers, respectively, where they undergo the overall electrochemical reactions:

$$\text{anode:}\quad CH_3OH + H_2O \rightarrow CO_2 + 6H^+ + 6e^- \tag{1}$$

$$\text{cathode:}\quad \tfrac{3}{2}O_2 + 6H^+ + 6e^- \rightarrow 3H_2O \tag{2}$$

with standard reduction potentials $E_a^0 = 0.02\,V$ and $E_c^0 = 1.23\,V$ vs. saturated hydrogen electrode (SHE), respectively. Due to methanol crossover, reaction (1) accounts indeed for methanol oxidation at both the anode and the cathode, while reaction (2) accounts for oxygen reduction at the cathode. The protons generated at the anode by reaction (1) diffuse across the polymer membrane, while the electrons pass as current through the external circuit to reach the cathode, where oxygen is reduced with the protons and the electrons to form water according to reaction (2). Globally, the two electrochemical reactions are combined to give the overall cell reaction:

$$CH_3OH + \tfrac{3}{2}O_2 \rightarrow CO_2 + 2H_2O \tag{3}$$

with standard cell potential $E_{cell}^0 = 1.21\,V$ at 298 K.

Among the performance controlling components of the direct methanol fuel cell, the anode electrode is known to be one of the most influential. In particular, the low activity of the electro-oxidation reaction of methanol is affected by the poisoning of the anode catalyst by stable adsorbed intermediates of methanol oxidation, which leads to large anodic overpotentials. Thus, in this paper we shall focus our attention on the anode side of the cell.

Most published papers on DMFC modeling consider Butler–Volmer or Tafel kinetics for the anodic reaction. However, the methanol electro-oxidation reaction (1) is known to be a multi-step reaction that takes place as several (possibly simultaneous) elementary steps at the molecular level, e.g., see Refs. [11,23] and references therein.

In contrast to most early DMFC models, Meyers and Newman [19] proposed a mechanistic model to describe complete

non-Tafel methanol oxidation kinetics on Pt–Ru catalysts based on the sequence of elementary steps proposed by Gasteiger et al. [24]. An interesting feature of their model is that it appropriately describes the transition from first-order kinetics for low methanol concentrations (high overpotentials) to zeroth-order kinetics for high methanol concentrations (low overpotentials), a transition first suggested by Ren et al. [25] and recently confirmed experimentally by Vidaković et al. [23].

Similar kinetic models have also been used by García et al. [8] and Kulikovsky [26] as improved models for the electrochemical oxidation of methanol. In all cases, the proposed kinetic expressions were used in the context of fully 1D, single-phase, DMFC models. Although multi-phase flow effects play an important role in the operation of DMFCs [15], in this paper the flow in the anode channels and gas diffusion layer is also described using the single-phase approximation, which leads to a simplified analytical description of the problem. Therefore, the aim of this paper is not to develop a mathematical model that fully describes all the phenomena that occur in a DMFC, but to illustrate the use a hybrid 3D/1D model that accounts for the electrochemical kinetics of Meyers and Newman [19].

Three-dimensional models constitute an excellent tool for exploring the spatial distribution of reactants and current density in the fuel cell. Thus, besides the overall cell polarization curves, we shall also study the spatial distribution of methanol in the anode channels, as well as the local distributions of current density, methanol crossover and fuel utilization at the anode catalyst layer, of interest for the optimized design of future-generation DMFCs.

The structure of the paper is as follows. The mathematical model is presented in Section 2; this comprises model assumptions (Section 2.1), description of the physical domain (Section 2.2), formulation of the 3D model (Section 2.3) and formulation of the 1D model (Section 2.4). The solution procedure is explained in Section 3, and the numerical results are presented in Section 4, including the validation of the model against experiments. Finally, the concluding remarks are presented in Section 5.

2. Mathematical model

2.1. Model assumptions

In the development of the mathematical model, a number of simplifying assumptions have been made. Some of them are central to our model, namely:

- Carbon dioxide produced at the anode is considered to be dilute enough to remain dissolved in the liquid phase, i.e. single-phase flow is considered in the anode.
- A large stoichiometric excess of air (or oxygen) is assumed in the cathode.

Strictly speaking, the first assumption restricts the validity of the model to the low current density regime, when the production of carbon dioxide at the anode is small. However, the single-phase model is expected to give correct parametric trends also in the high current density regime. A detailed study of two-phase flow and transport in DMFCs results in a much more complex modeling approach [15], which is not the aim of this paper. On the other hand, the second assumption, discussed in Section 2.4.1 below, allows us to impose a constant value for the oxygen ambient concentration along the cathode channel/flow distributor, further simplifying the analysis.

The rest of the assumptions, widely used in modeling studies of DMFCs, are the following:

- The flow is laminar and steady.
- The temperature is constant throughout the cell.
- The reactant concentrations are constant across the anode and cathode catalyst layers.
- The concentration of methanol is sufficiently small in the anode for the liquid phase to be a diluted methanol aqueous solution.
- The methanol that crosses over from the anode to the cathode is completely oxidized at the cathode catalyst layer.
- The effect of buoyancy in methanol transport is neglected.
- The membrane (assumed to be Nafion® 117) is fully hydrated and is impermeable to gases.
- The pressure gradient across the different cell layers is neglected.
- Ohmic losses in gas diffusion layers, channels and bipolar plates are neglected.

Some of this assumptions could be easily revised to incorporate additional effects in future extensions of the model, but will be maintained here for simplicity.

2.2. Physical domain

We shall assume a parallel channel geometry for the anode current collector. Accordingly, when describing the flow in a single channel we shall use periodic boundary conditions at the channel/rib mid-planes to reduce the computational cost. The investigation of the effect of geometry – including cross-section channel shape and/or flow channel geometry – on fuel cell performance should be considered in future work.

Fig. 1 shows an sketch of the physical domain considered here, which can be divided into seven regions:

(1) anode channel (ac);
(2) anode gas diffusion layer (agdl);
(3) anode catalyst layer (acl);
(4) polymer membrane (mem);
(5) cathode catalyst layer (ccl);
(6) cathode gas diffusion layer (cgdl);
(7) cathode channel (cc).

Since we are solving neither the electric field nor the temperature field, we omit from the computations both the anode current colector (acc) and the cathode current colector (ccc). The figure also shows the nomenclature used for the dimensions of the anode flow distributor (channel depth, δ_{ac}, channel width,

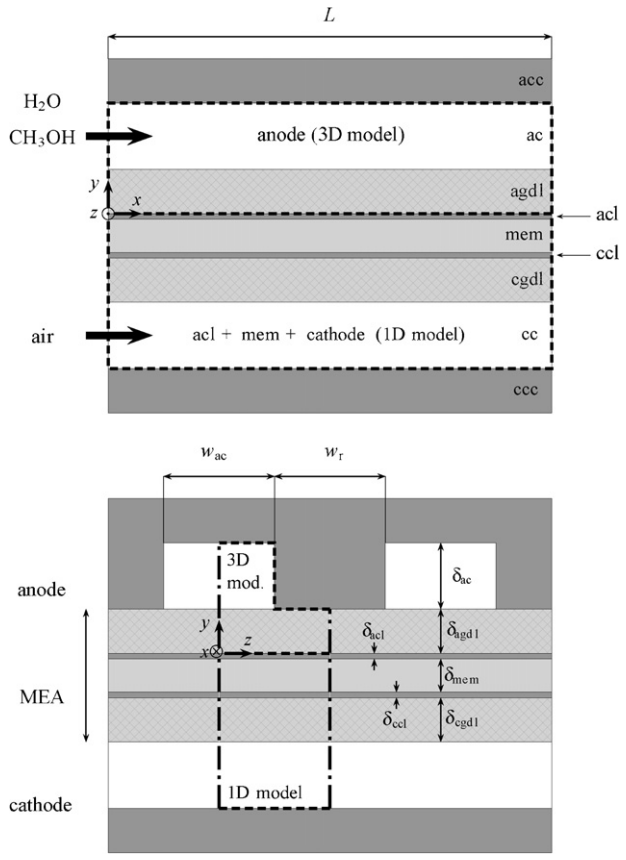

Fig. 1. Schematic of the modeling domains covered by the 1D and 3D models showing the coordinate system, and the notation used for the anode channel length, L, width, w_{ac}, depth, δ_{ac}, rib width w_r, and the thickness of the different layers of the MEA. Top: side view; bottom: cross-sectional view. The 1D model does not account for the detailed geometry of the cathode flow distributor.

w_{ac}, rib width, w_r) and the thickness of the different layers of the MEA.

2.3. 3D model (anode channel and gas diffusion layer)

The complete Navier–Stokes equations, complemented with the conservation equation for methanol, are solved in a three-dimensional (3D) domain with a control volume-based discretization to obtain the velocity and pressure distributions, as well as the concentration of methanol in the anode channel and gas diffusion layer.

2.3.1. Flow field

The Navier–Stokes and continuity equations governing the steady motion of an incompressible fluid of constant density and viscosity, ρ and μ, through an isotropic porous medium may be written as [27]:

$$\nabla \cdot \boldsymbol{u} = 0 \tag{4}$$

$$\frac{\rho}{\epsilon^2}(\boldsymbol{u}\cdot\nabla)\boldsymbol{u} = -\nabla p + \frac{\mu}{\epsilon}\nabla^2\boldsymbol{u} + \boldsymbol{S}_u \tag{5}$$

in terms of the porosity ϵ of the porous matrix. Here we shall use the value $\epsilon_{agdl} = 0.6$ for the porosity of the anode gas diffusion layer, while we simply set $\epsilon = 1$ in the anode channel, thus reducing (4) and (5) to the usual Navier–Stokes equations. In writing the above equations we have used the superficial velocity, $\boldsymbol{u}$, based on the volumetric flow rate, and we have neglected buoyancy effects. Since we will incorporate the effect of the electrochemical reactions as boundary conditions at the anode gas diffusion layer/catalyst interface, we also assume that there are no mass sources or sinks associated with the electrochemical reactions inside the computational domain.

As discussed in Section 2.1, we consider that the concentration of methanol in the anode channel is so small that it does not alter significantly the physical properties of water. Accordingly, ρ and μ represent the effective density and viscosity of water, given in Refs. [28,29] as

$$\rho = 1000 - 0.0178(T - 277.15)^{1.7} \ \ (\mathrm{kg\,m^{-3}}) \tag{6}$$

$$\mu = 0.458509 - 5.30474\times10^{-3}T + 2.31231\times10^{-5}T^2 - 4.49161\times10^{-8}T^3 + 3.27681\times10^{-11}T^4 \ \ (\mathrm{kg\,m^{-1}\,s^{-1}}) \tag{7}$$

in terms of the temperature T of operation, which here denotes the absolute (Kelvin) temperature.

The laminar flow in the porous gas diffusion layer is modeled by the addition of a momentum source in the governing momentum equation:

$$\boldsymbol{S}_u = -\left(\frac{\mu}{K}\right)\boldsymbol{u} \tag{8}$$

where K is the isotropic permeability of the medium. Note that for the typically small values of the permeability K of the porous regions of fuel cell electrodes (we use $K = 10^{-12}\,\mathrm{m^2}$) the addition of this source term simply reduces (5) to Darcy's Law. The source term, representing the extra resistance force suffered by the fluid due to the presence of the porous medium, vanishes at the anode channel.

2.3.2. Methanol distribution

Due to the small methanol concentration in the anode of a DMFC, the velocity field, $\boldsymbol{u}$, is decoupled from the methanol concentration field, C_m, which is governed by the convection/diffusion equation:

$$\nabla\cdot(\boldsymbol{u}C_m) = D_m^{eff}\nabla^2 C_m \tag{9}$$

where D_m^{eff} is the effective diffusion coefficient of methanol in water, given by Yaws [30]:

$$D_m^{eff} = \begin{cases} D_{m,ac}^{eff} = 10^{-5.4163-999.787/T}\ \mathrm{m^2\,s^{-1}} \\ D_{m,agdl}^{eff} = \epsilon_{agdl}^{1.5} D_{m,ac}^{eff} \end{cases} \tag{10}$$

at the anode channel and gas diffusion layer, respectively. As can be seen, in the second expression we use the Bruggeman correction factor to take into account the extra resistance to diffusion of the porous medium.

2.3.3. Boundary conditions

Eqs. (4), (5), and (9) must be integrated supplemented with appropriate conditions on the boundaries of the 3D domain

shown in Fig. 1. At the non-permeable channel walls we prescribe non-slip and zero gradient boundary conditions for the velocity and concentration fields, respectively:

$$\boldsymbol{u} = \boldsymbol{0}, \qquad \boldsymbol{n} \cdot \nabla C_{\mathrm{m}} = 0 \tag{11}$$

where $\boldsymbol{n}$ is the outward normal vector and $\nabla = \partial/\partial x\, \boldsymbol{e}_x + \partial/\partial z\, \boldsymbol{e}_z + \partial/\partial z\, \boldsymbol{e}_z$ is the gradient operator. At the inlet of the anode flow channel we specify the velocity and methanol concentration:

$$\boldsymbol{u} = U_{\mathrm{in}} \boldsymbol{e}_x, \qquad C_{\mathrm{m}} = C_{\mathrm{m,in}} \tag{12}$$

while at the symmetry planes and channel exit we set zero gradient boundary conditions for both the velocity and concentration fields:

$$\boldsymbol{n} \cdot \nabla \boldsymbol{u} = \boldsymbol{0}, \qquad \boldsymbol{n} \cdot \nabla C_{\mathrm{m}} = 0 \tag{13}$$

At the porous portion of the inlet and outlet boundaries a zero gradient boundary condition is prescribed for both pressure and methanol concentration. The internal boundary condition at the anode channel/gas diffusion layer interface is appropriately handled by imposing the continuity of flux and scalar variables.

The only non-trivial boundary condition is that imposed at the anode gas diffusion layer/catalyst interface, where we prescribe the molar flux of methanol:

$$(\boldsymbol{u}\, C_{\mathrm{m}} - D_{\mathrm{m}}^{\mathrm{eff}} \nabla C_{\mathrm{m}})\Big|_{y=0} \cdot \boldsymbol{n} = N_{\mathrm{m}} \tag{14}$$

which is due to methanol crossover and to the methanol consumption by the anodic reaction, and the normal velocity:

$$\boldsymbol{u}|_{y=0} \cdot \boldsymbol{n} = \left(n_{\mathrm{d}}^{\mathrm{w}} + \frac{1}{6}\right) \frac{i}{F} \frac{W_{\mathrm{w}}}{\rho} \tag{15}$$

which is due to the electro-osmotic flux of water across the membrane and to the water consumption by the anodic reaction – both proportional to the local current density i generated at the anodic reaction. Here F is Faraday's constant and W_{w} is the molecular weight of water. The electro-osmotic drag coefficient of water $n_{\mathrm{d}}^{\mathrm{w}}$ appearing in (15) is defined as the number of water molecules dragged by a hydrogen ion moving in the membrane, and is given by Guo and Ma [13]:

$$n_{\mathrm{d}}^{\mathrm{w}} = 2.9 \exp\left[1029 \left(\frac{1}{333} - \frac{1}{T}\right)\right] \tag{16}$$

It is important to note that the local molar flux of methanol at the catalyst layer, N_{m}, and the local current density, i, that appear on the right hand side of Eqs. (14) and (15), are not known a priori. The purpose of the 1D model presented below is precisely to calculate the values of N_{m} and i at the active boundary from the analysis of the remaining elements of the cell, namely the membrane, the catalyst layers, and the cathode flow field, thereby closing the mathematical problem.

2.4. 1D model (MEA and cathode)

The 3D mathematical model for the anode flow field described above will be complemented with a one-dimensional (1D) across-the-membrane model that provides the local values of the molar flux of methanol, N_{m}, and current density, i, at the active boundary in terms of the cell voltage, V, and the local methanol concentration there, $C_{\mathrm{m,acl}} \equiv C_{\mathrm{m}}|_{y=0}$. As previously discussed, this 1D model, including both catalyst layers, the membrane, and the cathode flow field, will allow us to close the mathematical problem through Eqs. (14) and (15).

2.4.1. Transport of O_2 in the cathode

Unlike ordinary polymer exchange membrane fuel cells, DMFCs are known to suffer from mass transport limitations mostly at the anode [3]. As a consequence, the anode flow field design turns out to be a key element for the optimal operation of DMFCs [31]. In fact, with proper control of water crossover to avoid cathode flooding, oxygen transport in the cathode is typically sufficient to sustain the – usually low – current densities generated in DMFCs, even in the case of air-breathing DMFC stacks [32]. This is especially true in the low current density regime, for which our single-phase model is expected to give the best results.

To reduce the computational cost, we shall circumvent the analysis of the cathode flow field by introducing an overall mass-transfer coefficient to model the transport of O_2 from the ambient air to the cathode catalyst layer. Thus, we simply write the molar flux of oxygen that reaches the cathode catalyst layer as

$$N_{\mathrm{O_2}} = \alpha_2 (C_{\mathrm{O_2,amb}} - C_{\mathrm{O_2,ccl}}) \tag{17}$$

in terms of a mass-transfer coefficient

$$\alpha_2 = \left(\frac{1}{h_{\mathrm{O_2}}} + \frac{\delta_{\mathrm{cgdl}}}{D_{\mathrm{O_2,cgdl}}^{\mathrm{eff}}}\right)^{-1} \tag{18}$$

that includes both the convective and diffusive transport losses through the mass transfer resistances $h_{\mathrm{O_2}}$ and $D_{\mathrm{O_2,cgdl}}^{\mathrm{eff}}/\delta_{\mathrm{cgdl}}$, respectively.

In the above expression, δ_{cgdl} is the thickness of the cathode gas diffusion layer and, using the Bruggeman correction factor, we write the effective diffusivity of oxygen in the cathode gas diffusion layer as

$$D_{\mathrm{O_2,cgdl}}^{\mathrm{eff}} = \epsilon_{\mathrm{cgdl}}^{1.5} D_{\mathrm{O_2,air}} \tag{19}$$

where ϵ_{cgdl} is the porosity of the porous matrix, and

$$D_{\mathrm{O_2,air}} = D_{\mathrm{O_2,air}}^{\mathrm{ref}} \left(\frac{T}{298}\right)^{3/2} \left(\frac{P_{\mathrm{amb}}}{P}\right) \tag{20}$$

is the diffusivity of oxygen in air, expressed in terms of its reference value $D_{\mathrm{O_2,air}}^{\mathrm{ref}}$ at 298 K and 1 atm, given in Table 1.

It is worth noting that when imposing a constant value $C_{\mathrm{O_2,amb}}$ for the oxygen "ambient" concentration along the cathode channel/flow distributor, a large stoichiometric excess of air (or oxygen) is being implicitly assumed. To be consistent with this approximation, we shall also neglect the convective loses ($h_{\mathrm{O_2}} \simeq \infty$) when evaluating the molar flux of oxygen reaching the cathode catalyst layer. Nevertheless, in real devices water flooding may obstruct oxygen transport in the cathode resulting in smaller values of $h_{\mathrm{O_2}}$ and $D_{\mathrm{O_2,cgdl}}^{\mathrm{eff}}$ (and therefore of α_2) than

Table 1
Physical constants and design parameters involved in the 3D model for the anode channel (ac) + gas diffusion layer (agdl).

Parameter	Physical description	Value	Reference
F	Faraday's constant	96485 C mol^{-1}	–
W_m	Molecular weight of methanol	0.032 kg mol^{-1}	–
W_w	Molecular weight of water	0.018 kg mol^{-1}	–
ϵ_{ac}	Porosity of ac	1	–
ϵ_{agdl}	Porosity of agdl	0.6	Assumed
K_{ac}	Permeability of ac	∞	–
K_{agdl}	Permeability of agdl	10^{-12}	Assumed
L	Anode channel length	8×10^{-2} m	Assumed
w_{ac}	Anode channel width	1.5×10^{-3} m	Assumed
δ_{ac}	Anode channel depth	1×10^{-3} m	Assumed
w_r	Anode land width	1×10^{-3} m	Assumed
δ_{agdl}	Thickness of the agdl	1.5×10^{-4} m	Assumed

those considered here. This could lead, mostly for high current densities, to mass transfer limitations at the cathode that are not included in this simplified model.

2.4.2. Mass balance of O_2 at the cathode catalyst layer

The oxygen that reaches the cathode catalyst layer either combines with the electrons and protons, or reacts directly with the methanol that crosses the membrane, to form water according to reactions (2) and (3), respectively. Accordingly, the mass balance of O_2 at the cathode catalyst layer can be written as

$$N_{O_2} = \frac{i}{4F} + \frac{3}{2}N_{cross} \tag{21}$$

with N_{cross} and i given by Eqs. (23) and (27) below, respectively.

2.4.3. Mass balance of methanol at the anode catalyst layer

Similarly, the methanol that reaches the anode catalyst layer by convection and diffusion from the anode backing layer must equal the amount of methanol consumed at the catalyst layer by reaction (1) plus the molar flux of methanol that permeates through the membrane, according to

$$N_m = \frac{i}{6F} + N_{cross} \tag{22}$$

with N_{cross} and i given by Eqs. (23) and (30), respectively.

2.4.4. Methanol crossover

Methanol transport across the membrane is driven by molecular diffusion, pressure gradient and electro-osmotic drag [2]. However, the effect of pressure gradient is typically small and can be neglected in the first approximation [15]. Then, assuming Fickian diffusion for methanol in the membrane, the molar flux of methanol can be written as

$$N_{cross} = n_d^m \frac{i}{F} - D_{m,mem}^{eff} \left.\frac{dC_m}{dy}\right|_{mem} \tag{23}$$

where n_d^m is the electroosmotic drag coefficient of methanol, defined as the number of methanol molecules dragged by a hydrogen ion moving in the membrane, and $D_{m,mem}^{eff}$ is the effective diffusion coefficient of methanol in the membrane (Nafion® 117) assumed to be independent of the concentration, which is a good approximation for the low methanol concentrations that we shall consider here.

The electroosmotic drag coefficient of methanol is given by Ren et al. [33]:

$$n_d^m = \frac{W_w}{\rho_w} n_d^w C_{m,acl} \tag{24}$$

in terms of the electro-osmotic drag coefficient of water, n_d^w, defined in Eq. (16) above.

Although there are different expressions available in the literature for the effective diffusion coefficient of methanol in the membrane (see, e.g., the discussion given in Ref. [34]), we choose that given by Scott et al. [1]:

$$D_{m,mem}^{eff} = 4.9 \times 10^{-10} \exp\left[2436\left(\frac{1}{333} - \frac{1}{T}\right)\right] \quad (m^2\,s^{-1}) \tag{25}$$

which roughly corresponds to the temperature range covered in this study, 298 K $\lesssim T \lesssim$ 363 K.

Due to the fast oxidation of methanol in the cathode, the resulting methanol concentration at the cathode catalyst layer, $C_{m,ccl}$, is very small, and can be considered to be zero in the first approximation. Accordingly, the diffusive flux of methanol in (23) can be approximated as

$$-D_{m,mem}^{eff} \left.\frac{dC_m}{dy}\right|_{mem} \simeq D_{m,mem}^{eff} \frac{C_{m,acl}}{\delta_{mem}} \tag{26}$$

where δ_{mem} is the thickness of the membrane. In a conventional cell δ_{mem} is typically small compared to the channel width and length. Consequently, the methanol concentration gradients across the membrane (i.e. in the y-direction as defined in Fig. 1) are anticipated to be large compared to those in the x- and z-directions. Thus, the flux of methanol through the membrane is mainly determined by the local value of the methanol concentration at the anode catalyst layer $C_{m,acl}$, as implicitly stated by Eqs. (23) and (26).

2.4.5. Electrochemical reduction of O_2 in the cathode

We shall assume that the electrochemical reduction of oxygen at the cathode follows Tafel kinetics with first order dependence in oxygen concentration:

$$i + i_p = \delta_{ccl}(ai_0)_c \frac{C_{O_2,ccl}}{C_{O_2,ref}} \exp\left(\frac{\alpha_c F}{RT}\eta_c\right) \tag{27}$$

where

$$i_p = 6FN_{cross} \tag{28}$$

is the parasitic current density due to the permeability of the membrane to methanol, i.e. the current that would be generated by the methanol that crosses-over the membrane, δ_{ccl} is the thickness of the cathode catalyst layer, a_c is the effective cathodic catalyst surface area per unit volume, $C_{O_2,ccl}$ is the molar concentration of oxygen at the catalyst layer, α_c is the cathode transfer coefficient, and $i_{0,c}$ is the exchange current density of the cathodic reaction, given as a function of T by Wang

and Wang [15]:

$$i_{0,c} = i_{0,c}^{ref} \exp\left[\frac{73200}{R}\left(\frac{1}{353} - \frac{1}{T}\right)\right] \quad (29)$$

in terms of its reference value $i_{0,c}^{ref}$ at 353 K.

2.4.6. Electrochemical oxidation of methanol in the anode

In this study, we adopt the Meyers and Newman [19] kinetic model for the oxidation of methanol on Pt–Ru catalysts:

$$i = \delta_{acl}(ai_0)_a \frac{\kappa\, C_{m,acl} \exp(\alpha_a F/RT\eta_a)}{C_{m,acl} + \lambda \exp(\alpha_a F/RT\eta_a)} \quad (30)$$

where δ_{acl} is the thickness of the anode catalyst layer, a_a is the effective anodic catalyst surface area per unit volume, $i_{0,a}$ is the exchange current density of the anodic reaction, $C_{m,acl}$ is the molar concentration of methanol at the catalyst layer, α_a is the anode transfer coefficient, and κ and λ are two experimentally fitted coefficients [8].

In the above expression, the anode exchange current density is given by Wang and Wang [15]:

$$i_{0,a} = i_{0,a}^{ref} \exp\left[\frac{35570}{R}\left(\frac{1}{353} - \frac{1}{T}\right)\right] \quad (31)$$

in terms of its reference value $i_{0,a}^{ref}$ at 353 K, and the molar methanol concentration, $C_{m,acl}$, is assumed to be uniform across the catalyst layer, a condition that is generally satisfied due to the small thickness of the catalyst layer and the high rate of methanol transport across it [26].

The kinetic model (30) was derived by Meyers and Newman [19] assuming complete methanol oxidation. Similar expressions have been recently used by García et al. [8] and Kulikovsky [26] as improved models for methanol electro-oxidation, a process that is known to deviate significatively from Tafel kinetics. In both cases, Eq. (30) was used in the context of fully 1D models.

As previously discussed, Eq. (30) describes the transition from first-order kinetics for low methanol concentrations and high overpotentials to zeroth-order kinetics for high methanol concentrations and low overpotentials. According to Meyers and Newman [19], the reason for this transition is that the rate of electrochemical oxidation of methanol is mainly determined by the desorption of the reactive molecules from the catalyst surface, except for sufficiently low methanol concentrations (i.e. high current densities), when the diffusive transport to the catalyst surface becomes the rate-determining step.

As a consequence, the above kinetic model can also be derived from a simple two-step reaction mechanism that accounts for a slow potential-independent step of methanol adsorption on the catalyst layer, coupled to a second step with Tafel kinetics corresponding to the electrochemical conversion of the adsorbed species [26].

It should be emphasized that the above kinetic expression (30) avoids the use of nonintuitive transitions between different reaction orders at certain threshold concentrations. In particular, it shows that the threshold concentration depends on the anodic overpotential according to $C_{m,acl}^{thres} \sim \lambda \exp(\alpha_a F\eta_a/RT)$, and therefore cannot be taken as constant, as done in previous work [15].

2.4.7. Equation for the cell voltage

The cell voltage V is determined by the equation:

$$V = E_{cell} - \eta_a - \eta_c - i\frac{\delta_{mem}}{\sigma_{mem}} \quad (32)$$

where E_{cell} is the ideal electromotive force of the cell, η_a and η_c are the anodic and cathodic overpotentials, respectively, and the last term represents the ohmic drop across the membrane, expressed here in terms of the local current density, i, the thickness of the membrane, δ_{mem}, and the ionic conductivity of the membrane, σ_{mem}, assumed to be a constant, since the membrane is fully hydrated in liquid-feed DMFCs.

The ideal electromotive force of the cell is given by Scott et al. [1]:

$$E_{cell} = E_{cell}^0 + (T - T_0)\left(\frac{\partial E}{\partial T}\right)_{liq} - \frac{\Delta N}{n}\frac{RT}{F}\log\left(\frac{P}{P_{amb}}\right) \quad (33)$$

where E_{cell}^0 is the ideal electromotive force under standard conditions, i.e. $C_m = 1000\,mol\,m^{-3}$, $P_{amb} = 1\,atm$, $T = 298\,K$, $(\partial E/\partial T)_{liq}$ is the rate of change of E_{cell} with T, and the last term represents the effect of pressure in the cathode potential. We shall assume here that the methanol and water of the overall reaction are liquid, hence $\Delta N/n = -0.5/2$.

Finally, the membrane (Nafion® 117) conductivity is given by Scott et al. [1]:

$$\sigma_{mem} = \sigma_{mem}^0 \exp\left[1268\left(\frac{1}{298} - \frac{1}{T}\right)\right] \quad (34)$$

in terms of the temperature T of operation, where σ_{mem}^0 is the reference ionic conductivity of the membrane at 298 K.

3. Solution procedure

3.1. Solution of the 1D model

Although the nonlinear character of the equations involved in the 1D model precludes an analytical solution of the problem, a numerical solution can be easily obtained using iterative methods.

Assume that we are given the local values of $C_{m,acl}$ and V at the anode catalyst layer. These will be provided at every iteration by the numerical solution of the 3D anode model. Then, appropriate manipulations of Eqs. (17), (21)–(23), (27), (28), and (30) yield the following set of analytic expressions for the unknowns i, η_c, η_a, N_{cross}, i_p, N_{O_2}, and $C_{O_2,ccl}$ as a function of N_m and $C_{m,acl}$:

$$i(N_m, C_{m,acl}) = 6F\left[\frac{N_m - C_{m,acl}D_{m,mem}^{eff}/\delta_{mem}}{1 + 6n_d^m(C_{m,acl})}\right] \quad (35)$$

$$\eta_c(N_m, C_{m,acl}) = \frac{RT}{\alpha_c F}\ln\left[\frac{6FN_mC_{O_2,ref}}{\delta_{ccl}(ai_0)_c\, C_{O_2,ccl}(N_m, C_{m,acl})}\right] \quad (36)$$

$$\eta_a(N_m, C_{m,acl}) = \frac{RT}{\alpha_a F} \ln\left[\frac{C_{m,acl}\, i(N_m, C_{m,acl})}{\delta_{acl}(ai_0)_a\, \kappa\, C_{m,acl} - \lambda\, i(N_m, C_{m,acl})}\right] \quad (37)$$

$$N_{cross}(N_m, C_{m,acl}) = N_m - \frac{i(N_m, C_{m,acl})}{6F} \quad (38)$$

$$i_p(N_m, C_{m,acl}) = 6F N_{cross}(N_m, C_{m,acl}) \quad (39)$$

$$N_{O_2}(N_m, C_{m,acl}) = \frac{3}{2} N_m \quad (40)$$

$$C_{O_2,ccl}(N_m, C_{m,acl}) = C_{O_2,amb} - \frac{3}{2}\frac{N_m}{\alpha_2} \quad (41)$$

where the electro-osmotic drag coefficient of methanol appearing in Eq. (35), $n_d^m(C_{m,acl})$, is given as a function of $C_{m,acl}$ by Eq. (24).

Substituting Eqs. (35)–(37) in (32) provides the following non-linear relationship between N_m, $C_{m,acl}$, and V:

$$f(N_m, C_{m,acl}) \equiv E_{cell} - V - \eta_a(N_m, C_{m,acl}) - \eta_c(N_m, C_{m,acl}) - i(N_m, C_{m,acl})\frac{\delta_{mem}}{\sigma_{mem}} = 0 \quad (42)$$

which can be readily solved for N_m using a Newton–Raphson method for given values of $C_{m,acl}$ and V. After solving for N_m, the remaining unknowns can be obtained from Eqs. (35)–(41).

For low methanol concentrations the denominator inside the logarithm of Eq. (37) approaches zero, yielding high anode overpotentials and complicating the numerical solution of Eq. (42). In this limit, we used as initial guess for N_m the asymptotic solution of Eq. (42) given in the Appendix, which proved to be a good technique to accelerate the convergence of the numerical method.

Illustrative results from the numerical solution of the 1D model are presented in Fig. 2. The local current density, i, is plotted together with the anodic and cathodic overpotentials, η_a and η_c, versus the local concentration of methanol at the active layer, $C_{m,acl}$, for different values of the cell voltage, V. As can be seen, for small methanol concentrations i grows linearly with $C_{m,acl}$, until it saturates for $C_{m,acl}^{thres} \sim \lambda \exp(\alpha_a F \eta_a / RT)$ due to non-Tafel effects. For higher methanol concentrations the current density decreases first due to methanol crossover (more prominent for low current densities and high cell voltages) and later to mass transport limitations at the cathode – as reflected by the sudden rise of the cathodic overpotential – until it eventually vanishes.

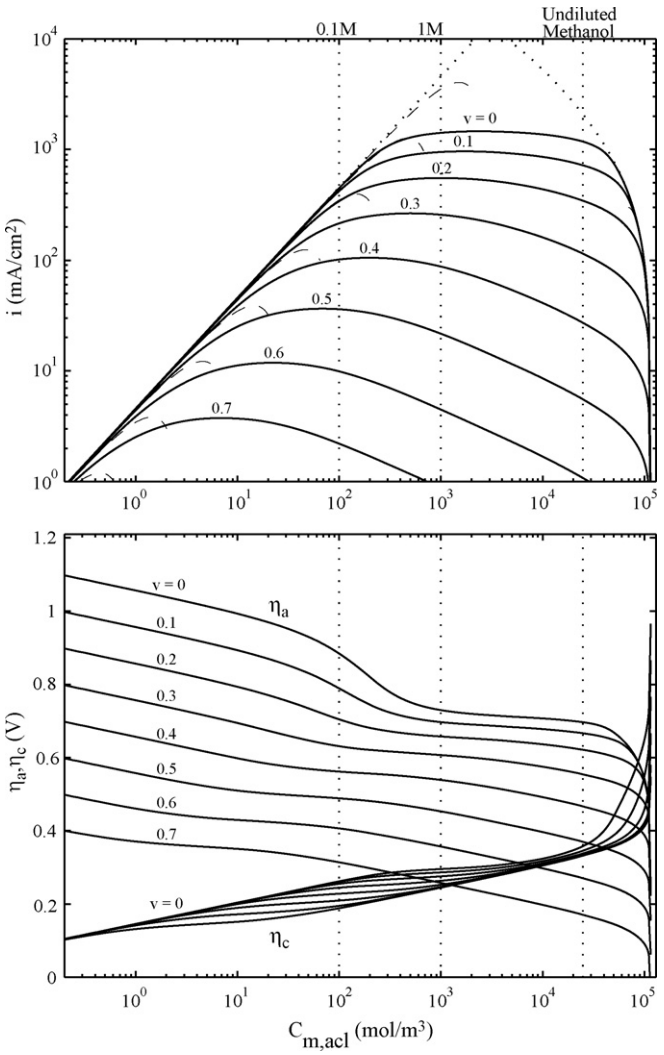

Fig. 2. Variation of the local current density i (upper plot), anode overpotential η_a, and cathode overpotential η_c (lower plot) with the local concentration of methanol at the anode catalyst layer, $C_{m,acl}$, for different cell voltages V (solid lines). Vertical dashed lines corresponding to 0.1 and 1 M methanol concentration and undiluted methanol are indicated for illustrative purposes. The dashed lines in the upper plot represent the asymptotic solution for small values of $C_{m,acl}$ given in the Appendix.

3.2. Numerical solution of the coupled 3D/1D model

For a fixed value of the cell voltage V, the coupled 3D/1D model was solved using the commercial finite-volume-based CFD code FLUENT®6.2. The computational domain was discretized using a Cartesian-structured grid generated with GAMBIT® 2.0. The total number of volume elements was 24,000 in the anode channel and 20,000 in the gas diffusion layer. To ensure a good resolution at the most critical regions, the grid points were clustered at the anode channel/gas diffusion layer interface and in the vicinity of the anode catalyst layer.

The boundary conditions at the gas diffusion layer/catalyst interface given by Eqs. (14) and (15) were implemented in FLUENT® through the use of user defined functions (UDFs). This allowed us to solve the 1D model at every iteration using the local value of C_m at the active boundary to obtain the corresponding molar flux of methanol N_m.

Once the numerical solution was converged, the average current density of the cell was calculated according to

$$I = \frac{1}{A_{acl}} \int_{\sigma_{acl}} i\, d\sigma \quad (43)$$

where the local current density i is given by Eq. (35) and the surface integral is extended over the whole surface area A_{acl} of

the anode catalyst layer. The average parasitic current density due to crossover, I_p, was calculated similarly. Then, another value of V was given and the process was repeated until the whole polarization curve was obtained.

To check the accuracy of the numerical solution, a grid-refinement study was performed. The refined grid was obtained by halving the node spacing in each coordinate direction, increasing by a factor of eight the total number of grid elements. The numerical results obtained with the refined grid showed relative errors smaller than 10^{-3} in the numerical evaluation of the average current density as compared to the coarser grid. Considering the inherent limitations of the model (in particular, the uncertainties in the physical parameters) this level of accuracy was considered to be appropriate. Using the coarse grid, the convergence of a single point in the polarization curve took about 30 min of CPU time using a Pentium IV processor at 2.67 GHz with 1 GB RAM.

3.3. Physicochemical parameters

In the development of the present model several parameters have been introduced, such as the effective diffusion coefficients, gas diffusion layer porosities, protonic conductivity in the membrane, anode/cathode transfer coefficients, exchange current densities, etc. Most of them were taken from the literature, as summarized in Tables 1 and 2.

As a final remark, it should be noted that some parameters do not enter individually in the model. Instead, they appear grouped together in products such as $\delta_{acl}(ai_0)_a\kappa$ or $\delta_{ccl}(ai_0)_c$. Accordingly, if we, for instance, increase the specific area while decreasing the thickness of the catalyst layers by the same amount, the results will remain unaltered.

4. Results and discussion

4.1. Case studies

The different cases under study are summarized in Table 3. Simulations were performed for different methanol feed concentrations, $C_{m,in}$, temperatures of operation, T, methanol flow rates, U_{in}, and cathode fluid—either ambient pressure air or pure oxygen. The reference case (Case 0) corresponds to the flow of a 0.5 M (500 mol/m^3) methanol dilution at 1 mm/s inlet velocity and 80 °C, using ambient pressure air as the cathode fluid.

4.2. Overall cell performance

Figs. 3–5 summarize the computed overall cell performance for the different cases under study, including polarization and power–current curves, average parasitic current density due to crossover, and fuel utilization $FU = 100 \times I/(I + I_p)\%$ – defined as the ratio of the electrochemically reacted fuel and total fuel used – as a function of cell current density. Different figures illustrate the effect of methanol feed concentration (Fig. 3, cases 0–3, 12), the effect of temperature (Fig. 4, cases 0, 4–7), and the effect of methanol flow rate (Fig. 5, cases 0, 8–11). Fig. 3 also shows the effect of using ambient pressure air or pure oxygen as cathode fluid.

Table 2
Physical constants, transport, kinetic and design parameters involved in the 1D model for the anode catalyst layer (acl) + membrane (mem) + cathode (ccl, cgdl, cc)

Parameter	Physical description	Value	Reference
F	Faraday's constant	96485 C mol^{-1}	–
R	Universal gas constant	8.31 J mol^{-1} K^{-1}	–
W_m	Molecular weigth of methanol	0.032 kg mol^{-1}	–
W_w	Molecular weigth of water	0.018 kg mol^{-1}	–
$D^{ref}_{O_2,air}$	Diffusivity of O_2 in air at 298 K	2.5×10^{-5} m^2 s^{-1}	Perry et al. [35]
$X_{O_2,amb}$	O_2 molar fraction in the cathode channel	0.21 (air) / 1 (pure O_2)	–
$C_{O_2,amb}$	O_2 molar concentration in the cathode channel	$X_{O_2,amb}P_{amb}/RT$	–
$C_{O_2,ref}$	Reference O_2 molar concentration	$0.21P_0/RT$ mol m^{-3}	–
P_0	Reference pressure for $C_{O_2,ref}$	10^5 Pa	–
P_{amb}	Ambient pressure	1.013×10^5 Pa	–
α_a	Anode transfer coefficient	0.5	Murgia et al. [7]
α_c	Cathode transfer coefficient	1.2	Murgia et al. [7]
a_a	Anode catalyst surface area per unit volume	6×10^4 m^{-1}	–
a_c	Cathode catalyst surface area per unit volume	6×10^4 m^{-1}	–
κ	Experimental constant	7.5×10^{-4}	García et al. [8]
λ	Experimental constant	2.8×10^{-3} mol m^{-3}	García et al. [8]
$i^{ref}_{0,a}$	Anode exchange current density at 353 K	94.25 A m^{-2}	Ren et al. [33]
$i^{ref}_{0,c}$	Cathode exchange current density at 353 K	0.04222 A m^{-2}	Wang and Wang [15]
σ^0_{mem}	Membrane (Nafion) conductivity at 298 K	7.3 S m^{-1}	Scott et al. [1]
E^0_{cell}	Open circuit voltage at 298 K	1.213 V	Wang and Wang [15]
$(\partial E/\partial T)_{liq}$	Rate of change of E^0_{cell} with T	-1.4×10^{-4} V K^{-1}	Scott et al. [1]
δ_{acl}	Thickness of the acl	3×10^{-5} m	Assumed
δ_{mem}	Thickness of the membrane	1.78×10^{-4} m	Assumed
δ_{ccl}	Thickness of the ccl	3×10^{-5} m	Assumed
δ_{cgdl}	Thickness of the cgdl	1.5×10^{-4} m	Assumed
ϵ_{cgdl}	Porosity of cgdl	0.6	Assumed

Table 3
Operational parameters for the different cases under study

Case no.	$C_{m,in}$ (mol m^{-3})	T (K)	U_{in} (mm s^{-1})	Cathode fluid
0 (reference)	**500**	**353**	**1**	**Air**
1	**1000**	353	1	Air
2	**250**	353	1	Air
3	**125**	353	1	Air
4	500	**363**	1	Air
5	500	**343**	1	Air
6	500	**333**	1	Air
7	500	**298**	1	Air
8	500	353	**0.5**	Air
9	500	353	**2**	Air
10	500	353	**4**	Air
11	500	353	**8**	Air
12	500	353	1	<CE:BOLD>O</CE:BOLD>$_2$

As can be observed, the model reproduces appropriately the parametric trends reported in the literature, predicting an increase in cell voltage (and therefore power output) for increasing inlet methanol concentration, temperature, and methanol flow rate. As illustrated in the inset of Fig. 3, this trend is reversed at low current densities, when the cell voltage drop due to methanol crossover is larger for higher methanol concentration.

Fig. 3 also shows that, within the limitations of the present model, the main effect of increasing oxygen concentration in the cathode by using pure oxygen ($X_{O_2,pure} = 1$) instead of air ($X_{O_2,air} = 0.21$) is to reduce the cathodic overpotential by a constant amount, which can be estimated approximately from Eq. (27) as

$$\Delta\eta_c \simeq -\frac{RT}{\alpha_c F}\log\frac{X_{O_2,pure}}{X_{O_2,air}} = -\frac{RT}{\alpha_c F}\log\frac{1}{0.21} = 0.0395V \quad (44)$$

at $T = 353$ K, independently of the cell current density. This effect rises the overall cell voltage, therefore increasing the cell power output, but does not affect the limiting current density, which in our simplified model is mainly determined by mass transport limitations at the anode.

The parasitic current due to cross-over predicted by the model shows also values and trends similar to those reported in the lit-

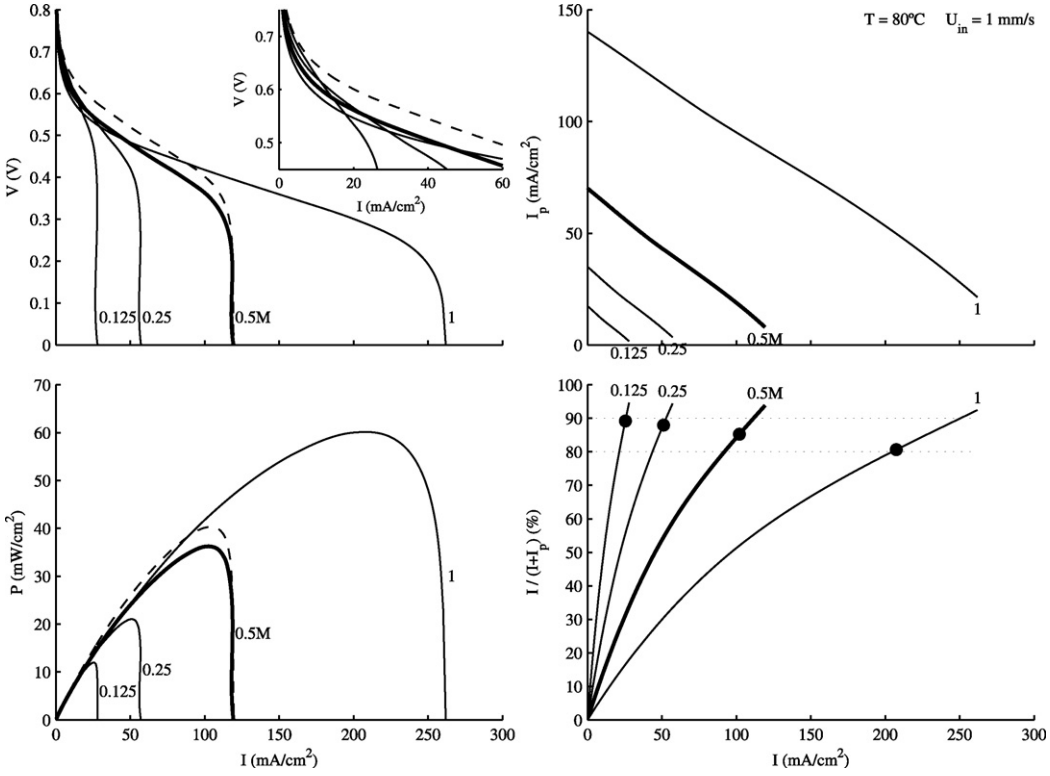

Fig. 3. Computed cell performance corresponding to $T = 80\,^{\circ}$C, $U_{in} = 1$ mm s^{-1}, and different methanol feed concentrations, $C_{m,in} = 0.125$, 0.25, 0.5, and 1 M (as indicated): polarization curve (upper left), power–current curve (lower left), average parasitic current density due to crossover (upper right), and fuel utilization % (lower right) as a function of cell current density. Cathode fluid: ambient pressure air (—), pure oxygen (– –) (shown only for $C_{m,in} = 0.5$ M). The solid dots in the lower right plot represent fuel utilization at maximum power.

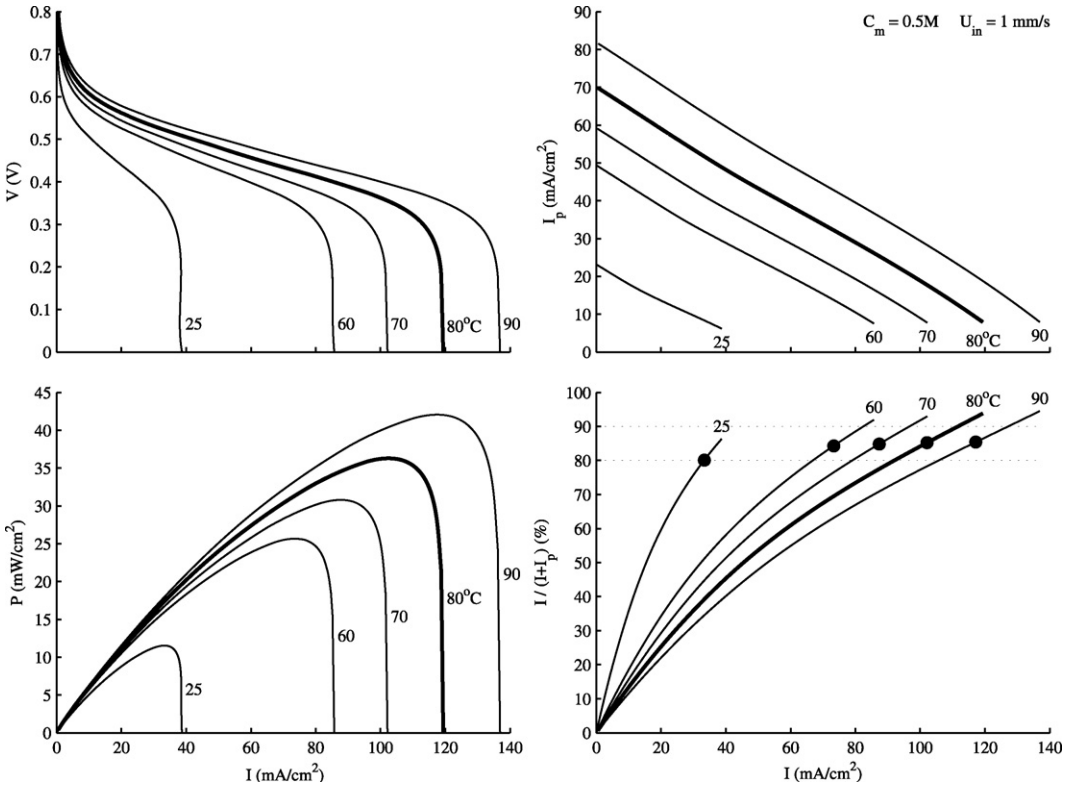

Fig. 4. Computed cell performance corresponding to $C_{m,in} = 0.5\,M$, $U_{in} = 1\,mm\,s^{-1}$, and different temperatures of operation, $T = 25$, 60, 70, 80, and 90 ° C (as indicated). See caption of Fig. 3 for details.

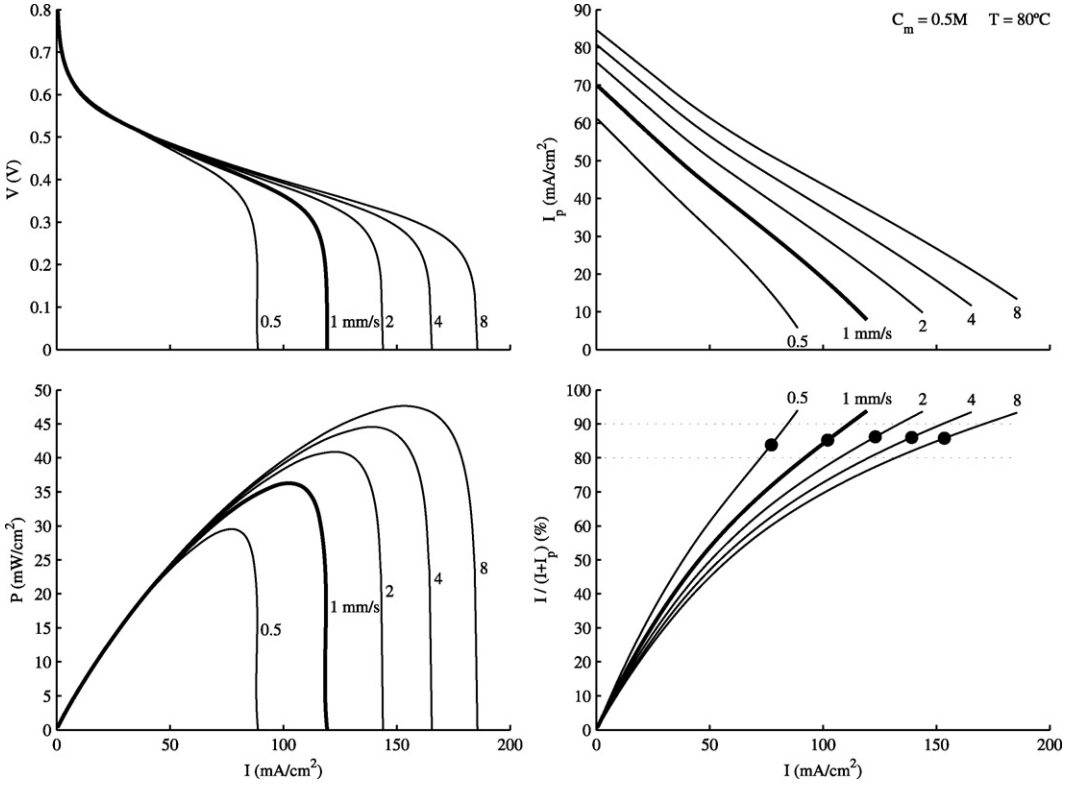

Fig. 5. Computed cell performance corresponding to $C_{m,in} = 0.5\,M$, $T = 80\,°C$, and different methanol feed velocities, $U_{in} = 0.5$, 1, 2, 4, and 8 $mm\,s^{-1}$ (as indicated). See caption of Fig. 3 for details.

erature [8,15]. Thus, the leakage current density decreases by operating the fuel cell at low methanol concentrations and low temperatures, and decreases almost linearly with cell current density. The results also show a reduction in parasitic current for low methanol flow rates. It is worth noting that even at the mass transport limited current density the model predicts a noticeable (i.e. non-zero) cross-over current, which is always larger than approximately 5% of the limiting current density (so that $FU_{max} \lesssim 95\%$).

It is also interesting to note that the fuel utilization at maximum power output, shown by solid dots in the lower right plot of each figure, reaches always values between 80 and 90%. These values, which increase with temperature and decrease with feeding methanol concentration, are also in agreement with previously reported results [25].

4.3. Methanol distribution in the anode

3D models constitute an excellent tool for exploring the spatial distribution of reactants and current density in the fuel cell. Figs. 6 and 7 show the distribution of methanol for the reference case at various cross-sections along the anode channel, at the channel symmetry plane, and at the anode gas diffusion layer/catalyst interface, corresponding to three different cell voltages: $V = 0.8$, 0.4 and 0 V. As expected, due to mass transport limitations the region below the current collector shows low methanol concentrations. Moreover, the methanol concentration at the catalyst layer is seen to decrease noticeably when increasing the cell current density, approaching a small – but finite – value at the limiting cell current density.

4.4. Anode flow field and water management

All the flows simulated herein exhibit Reynolds numbers of order unity based on the channel depth, δ_c, and methanol feed velocity, U, e.g., for the reference case $Re = \rho U \delta_c / \mu \simeq 2.7$. The flow is therefore steady and hydrodynamically developed over the entire channel, except for a short entry region of characteristic length $\delta_c \ll L$. Moreover, the water lost through the gas diffusion layer/catalyst interface, due to both electroosmotic drag and water consumption at the anodic reaction, reduces the volumetric flow of water as it evolves downstream.

For illustrative purposes, Fig. 8 shows the streamlines of the flow at the channel symmetry plane and porous backing layer. The streamlines, obtained numerically, correspond to the same operating conditions considered in the previous section, i.e. the

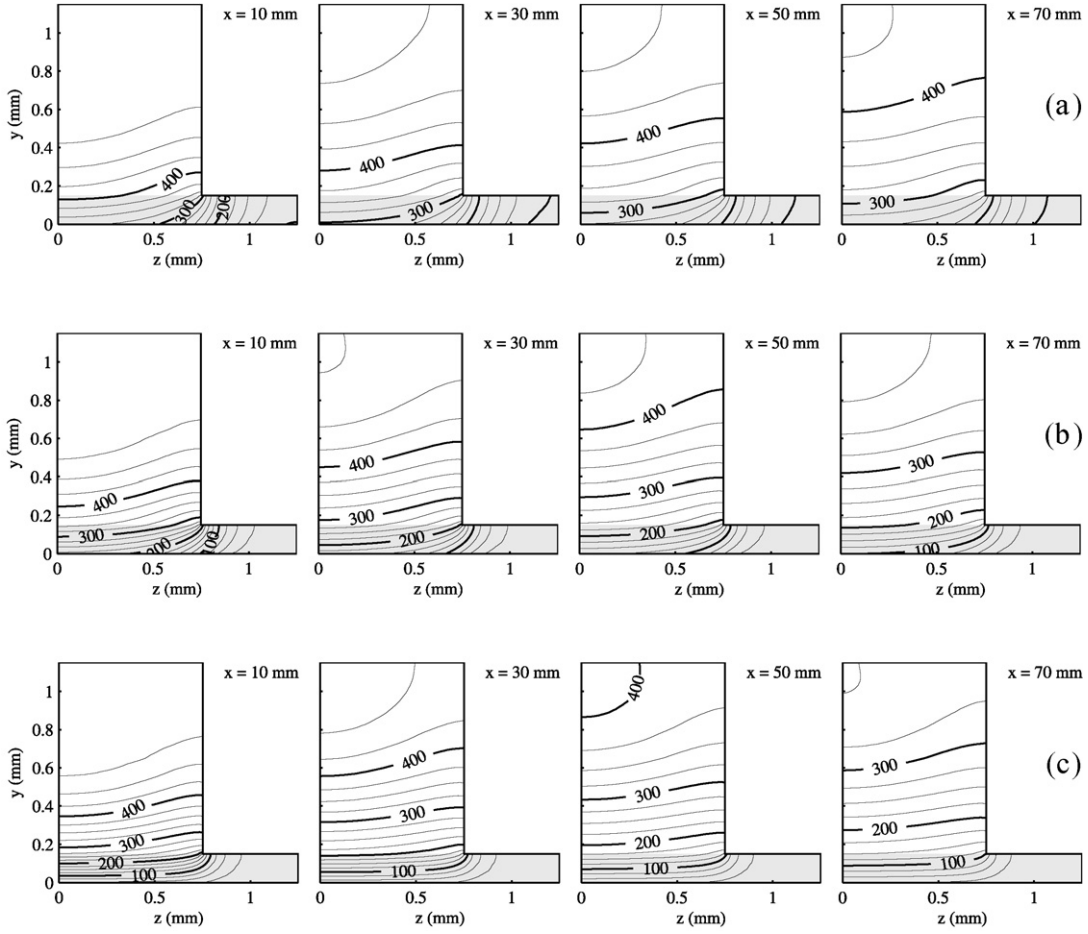

Fig. 6. Methanol concentration contours (mol m^{-3}) at various cross-sections along the anode channel ($x = 10$, 30, 50, and 70 mm, from left to right) corresponding to (a): $V = 0.8$ V, $I = 0.4$ mA cm^{-2}, (b): $V = 0.4$ V, $I = 85$ mA cm^{-2}, and (c): $V = 0$ V, $I = I_{max} = 119$ mA cm^{-2}. Results obtained for fixed values of $C_{m,in} = 500$ mol m^{-3} (0.5 M), $T = 80\,^{\circ}$C, and $U_{in} = 1$ mm s^{-1}. The shaded region represents the anode gas diffusion layer.

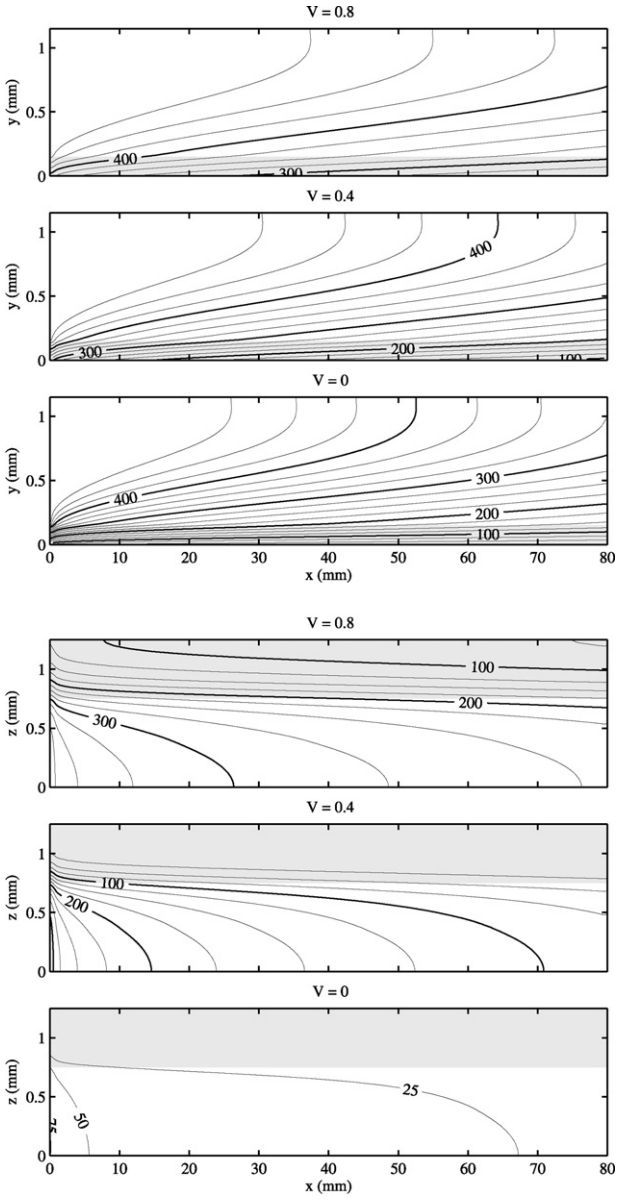

Fig. 7. Methanol concentration contours (mol m^{-3}) at the channel symmetry plane (upper plot) and gas diffusion layer/catalyst interface (lower plot) corresponding to the cases $V = 0.8$, 0.4, and 0 V shown in Fig. 6(a)–(c), respectively. The shaded region represents the anode gas diffusion layer (upper plot), and the region below the rib (lower plot).

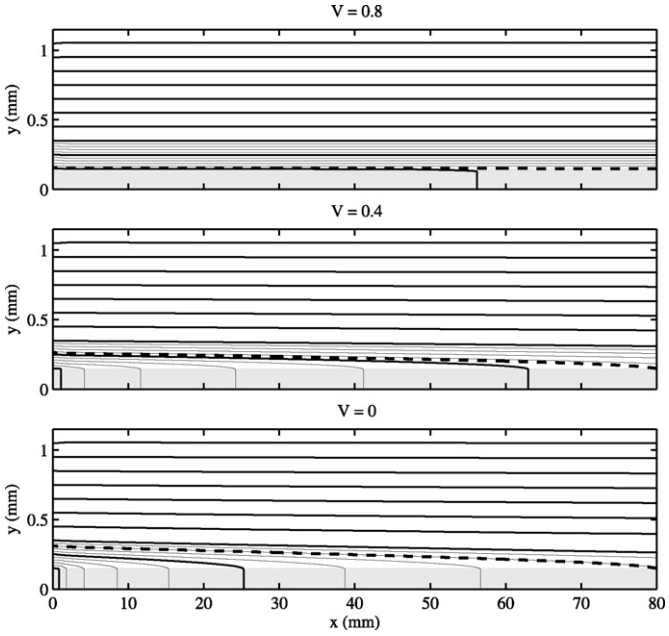

Fig. 8. Streamlines of the flow at the channel symmetry plane corresponding to the cases $V = 0.8$, 0.4, and 0 V shown in Figs. 6(a)–(c), respectively. The shaded region represents the anode gas diffusion layer, and the thick dashed line shows the dividing streamline.

reference case operating at $V = 0.8$, 0.4 and 0 V. In the plots, the shaded region represents the anode gas diffusion layer, while the thick dashed line shows the dividing streamline separating the fluid that exits the domain through the channel exit from that lost through the catalyst layer.

As should be expected, the fraction of fluid that is lost through the catalyst layer grows for increasing values of the cell current density, I, or decreasing cell voltages, V—in particular, the simulations reveal that about 6% of the inflow is lost for $V = 0.4$ V, and up to 10% for $V = 0$ V, i.e. at the cell limiting current density. For increasing values of the cell current density the diffusive transport of methanol through the porous layer becomes, therefore, more and more assisted by the convective transport of water towards the membrane, a mechanism that probably contributes to sustain higher limiting current densities. The numerical results reveal that the convective flow of water through the porous layer also contributes to the transverse transport of methanol to the region below the ribs, although this effect can not be seen in Fig. 8.

4.5. Current density, methanol crossover, and fuel utilization distributions in the anode catalyst layer

Fig. 9 shows the predicted distributions of current density, methanol crossover, and fuel utilization in the anode catalyst layer for the reference case, operating at $V = 0.4$ V, $I = 85$ mA/cm^2. As a consequence of the uneven distribution of methanol at the catalyst layer, the reaction occurs mainly below the gas channel, while the region below the current collector remains relatively inactive due to the low values of the methanol concentration there. On the other hand, the high methanol concentrations imposed near the inlet by the feeding stream induce high cross-over currents there, which locally lowers the fuel utilization.

4.6. Experimental validation of the numerical model

To validate the mathematical model we performed a series of simulations to compare the numerical results with the experimental data reported by Sundmacher et al. [18]. During the validation, the geometric parameters were varied from those in Table 1 so as to reproduce the experimental conditions in Ref. [18], namely: $L = 3 \times 10^{-2}$m, $w_{ac} = 2 \times 10^{-3}$m, $w_r = 1 \times 10^{-3}$ m, $\delta_{ac} = 2 \times 10^{-3}$ m, $\delta_{agdl} = \delta_{cgdl} = 0.3 \times 10^{-3}$ m, $\delta_{mem} = 0.178 \times 10^{-3}$ m. The operating conditions were also

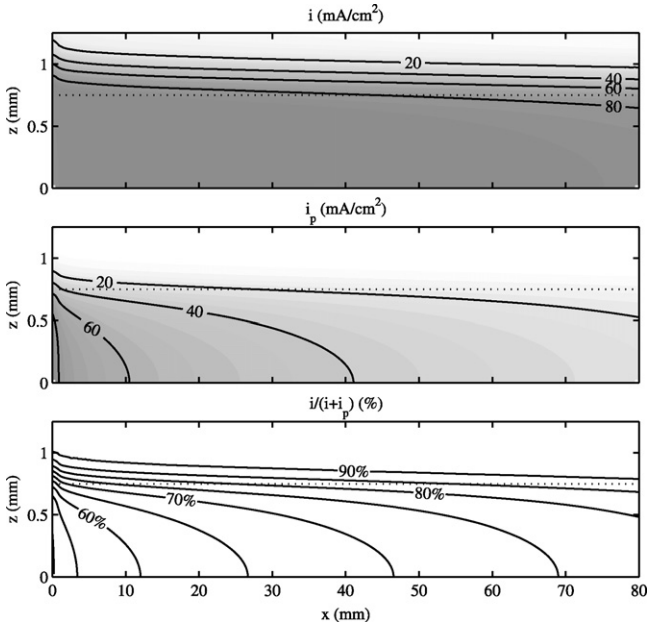

Fig. 9. Local distributions of the current density, i, methanol flux due to crossover, i_p, and fuel utilization, $i/(i+i_p)$, at the anode catalyst layer for the reference case, $C_{m,in} = 500\ mol\ m^{-3}$ (0.5 M), $T = 80\ ^\circ C$, $U_{in} = 1\ mm\ s^{-1}$, operating at $V = 0.4\ V$, $I = 85\ mA\ cm^{-2}$.

chosen so as to reproduce those in Ref. [18], i.e. $T = 343$ K, $U_{in} = 0.54$ mm/s, $P_{amb} = 2.5$ barg. The specific catalyst surface area, $a = 2 \times 10^4\ m^{-1}$, and the kinetic parameter, $\lambda = 1.25 \times 10^{-2}\ mol\ m^{-3}$, were also modified from the values shown in Table 1 in order to fit the experimental data.

Fig. 10 shows the experimental polarization curves given in Ref. [18] together with the numerical results provided by the mathematical model. As can be seen, the proposed model fits satisfactorily the experimental data in the low current density regime, where the cell voltage is mainly determined by activation polarization losses. However, multi-phase flow at both the anode and the cathode, which is not accounted for in this simplified model, may be partially responsible for the lack of quantitative agreement between experimental and numerical results for the high current densities reached for large methanol concentrations (2 M). Note, however, that even for the highest methanol feed concentrations the numerical results are very similar to those reported by Xu et al. [20] in the same parallel channel configuration.

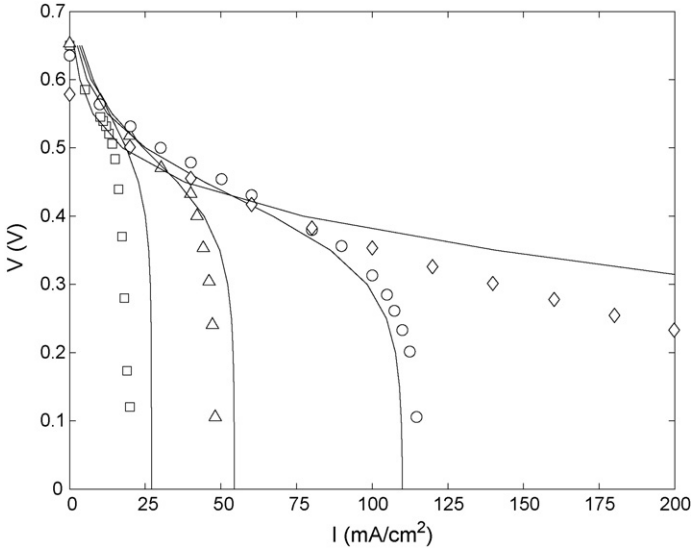

Fig. 10. Comparison of the experimental results reported by Sundmacher et al. [18](symbols) and the results provided by the mathematical model (solid lines) under similar operating conditions, for different methanol feed concentrations: (□) 0.125 M; (△) 0.25 M; (◯) 0.5 M; (◇) 2 M.

As a final remark, it is worth noting that the model results slightly overpredict the cell voltage for near open circuit conditions. The reason is that we are considering irreversible kinetic laws for both the electro-oxidation of methanol at the anode, Eq. (30), and the reduction of oxygen at the cathode, Eq. (27), while, indeed, for sufficiently low current densities the reverse reactions start to play a role. Accordingly, we can not expect the model to predict accurately open circuit voltages. A detailed account on the modeling and operation of a DMFC under open-circuit conditions can be found elsewhere [36,37].

5. Conclusions

A novel 3D/1D, isothermal, single-phase model has been developed for liquid-feed direct methanol fuel cells (DMFC). The mathematical model accounts for several physicochemical processes that limit the performance of DMFCs, namely the 3D convective/diffusive transport of methanol in the anode channel and gas diffusion layer, the parasitic electro-oxidation of methanol at the cathode due to methanol crossover, and the complex non-Tafel kinetics of methanol electro-oxidation at the anode, simulated using the kinetic model introduced by Meyers and Newman [19]. Although this model has been previously dismissed due to its complex non-linear nature [7], we were able to implement it in a computationally efficient way by using appropriate initial guesses based on asymptotic expansions.

When applied to the steady-state operation of a single cell DMFC with straight channels the model was able to predict methanol concentration distributions, polarization and power-current curves, local current density profiles, local and total water crossover, as well as effects of inlet temperature, methanol concentration and methanol flow rate.

The mathematical model was solved using a commercial CFD package, leading to polarization curves for different methanol feed concentrations, temperatures and volumetric methanol flow rate that are in agreement with the experimental results found in the literature.

Further model improvements, including multi-species transport, multi-phase flow, electronic and protonic potentials, and water and heat management are worth future investigation to improve the predictive capabilities of the complex physicochemical phenomena involved in liquid-feed DMFC.

Acknowledgements

The help of Francisco J. Sánchez-Cabo with the numerical implementation of the model is gratefully acknowledged. Use-

ful discussions with Drs. Antonio Revuelta and Bertrand Naud (CIEMAT) are also appreciated.

Appendix. Asymptotic solution of the 1D model in the limit of low methanol concentrations

The asymptotic solution to Eq. (42) in the limit $C_{\mathrm{m,acl}} \to 0$ is given by

$$N_{\mathrm{m}} \simeq N_{\mathrm{m}}^{\max} - \frac{\delta_{\mathrm{acl}}(a\,i_0)_{\mathrm{a}}\,\kappa}{6F\lambda^2} \times \left[\frac{6FC_{\mathrm{O_2,ref}}}{\delta_{\mathrm{ccl}}(a\,i_0)_{\mathrm{c}}\,C_{\mathrm{O_2,amb}}}\left(\frac{\delta_{\mathrm{acl}}(a\,i_0)_{\mathrm{a}}\,\kappa}{6F\lambda} + \frac{D_{\mathrm{m,mem}}^{\mathrm{eff}}}{\delta_{\mathrm{mem}}}\right)\right]^{\alpha_a/\alpha_b} \times C_{\mathrm{m,acl}}^{2+(\alpha_a/\alpha_b)} \exp\left[-\frac{\alpha_{\mathrm{a}}F}{RT}(E_{\mathrm{cell}} - V)\right] \quad (45)$$

where

$$N_{\mathrm{m}}^{\max} = \left[\frac{\delta_{\mathrm{acl}}(a\,i_0)_{\mathrm{a}}\,\kappa}{6F\lambda} + \frac{D_{\mathrm{m,mem}}^{\mathrm{eff}}}{\delta_{\mathrm{mem}}}\right] C_{\mathrm{m,acl}} + \left[\frac{\delta_{\mathrm{acl}}(a\,i_0)_{\mathrm{a}}\,\kappa}{F\lambda}\,\frac{W_{\mathrm{w}}n_{\mathrm{d}}^{\mathrm{w}}}{\rho_{\mathrm{w}}}\right] C_{\mathrm{m,acl}}^2 \quad (46)$$

is the maximum molar flux of methanol that can be sustained for a given methanol concentration. The expression for $N_{\mathrm{m}}^{\max}$ was obtained by equating to zero the denominator of the fraction inside the logarithm in Eq. (37). Notice that to reach the maximum flux of methanol the cell may require the application of negative voltages, which is impossible in practical devices where V must be always positive.

Once $N_{\mathrm{m}}^{\max}$ is known, the deviation of the molar flux of methanol below its maximum value can be calculated by substituting $N_{\mathrm{m}} = N_{\mathrm{m}}^{\max} - \Psi$ in Eqs. (35)–(41) and expanding (42) as an asymptotic series for small values of Ψ. The zeroth order term of the resulting expansion involves two logarithmic singularities, coming from (36) and (37), that must be counterbalanced by Ψ. Imposing that the zeroth order term must vanish in order to kill the logarithmic singularities, we obtain Eq. (45).

Finally from Eq. (35) we may write the local current density for small methanol concentrations as $i \simeq 6FN_{\mathrm{m}}$, with N_{m} given by Eq. (45).

References

[1] K. Scott, W.M. Taama, J. Cruickshank, J. Power Sources 65 (1997) 159–171.
[2] J. Cruickshank, K. Scott, J. Power Sources 70 (1998) 40–47.
[3] K. Scott, P. Argyropoulos, K. Sundmacher, J. Electroanal. Chem. 477 (1999) 97–110.
[4] S.F. Baxter, V.S. Battaglia, R.E. White, J. Electrochem. Soc. 146 (1999) 437–447.
[5] P. Argyropoulos, K. Scott, W.M. Taama, Chem. Eng. J. 78 (2000) 29–41.
[6] A.A. Kulikovsky, Electrochem. Commun. 4 (2002) 939–946.
[7] G. Murgia, L. Pisani, A.K. Shukla, K. Scott, J. Electrochem. Soc. 150 (2003) A1231–A1245.
[8] B.L. García, V.A. Sethuraman, J.W. Weidner, R.E. White, J. Fuel Cell Sci. Technol. 1 (2004) 43–48.
[9] R. Chen, T.S. Zhao, J. Power Sources 152 (2005) 122–130.
[10] A.A. Kulikovsky, J. Appl. Electrochem. 30 (2000) 1005–1014.
[11] J. Nordlund, G. Lindbergh, J. Electrochem. Soc. 149 (2002) A1107–A1113.
[12] F. Birgersson, J. Nordlund, H. Eksrtöm, M. Vynnycky, G. Lindbergh, J. Electrochem. Soc. 150 (2003) A1368–A1376.
[13] H. Guo, C.F. Ma, Electrochem. Commun. 6 (2004) 306–312.
[14] J. Ge, H. Liu, J. Power Sources 160 (2006) 413–421.
[15] Z.H. Wang, C.Y. Wang, J. Electrochem. Soc. 150 (2003) A508–A519.
[16] J. Divisek, J. Fuhrmann, K. Gartner, R. Jung, J. Electrochem. Soc. 150 (2003) A811–A825.
[17] V.A. Danilov, J. Lim, I. Moon, H. Chang, J. Power Sources 162 (2006) 992–1002.
[18] K. Sundmacher, T. Schultz, S. Zhou, K. Scott, M. Ginkel, E.D. Gilles, Chem. Eng. Sci. 56 (2001) 333–341.
[19] J.P. Meyers, J. Newman, J. Electrochem. Soc. 149 (2002) A718–A728.
[20] C. Xu, P.M. Follmann, L.T. Biegler, M.S. Jhon, Comp. Chem. Eng. 29 (2005) 1849–1860.
[21] G. Lu, C.Y. Wang, B. Sundén, M. Faghri, Transport Phenomena in Fuel Cells, WIT Press, Southampton, 2005, pp. 317–358.
[22] R. Sousa, E.R. Gonzalez, J. Power Sources 147 (2005) 32–45.
[23] T. Vidakovic, M. Christov, K. Sundmacher, J. Electroanal. Chem. 580 (2005) 105–121.
[24] H.A. Gasteiger, N. Marković, P.N. Ross, J. Cairns Jr., J. Phys. Chem. 97 (1993) 12020–12029.
[25] X. Ren, P. Zelenay, S. Thomas, J. Davey, S. Gottesfeld, J. Power Sources 86 (2000) 111–116.
[26] A.A. Kulikovsky, Electrochem. Commun. 7 (2005) 969–975.
[27] L. Ma, D.B. Ingham, M. Pourkashanian, D.B. Ingham, I. Pop, Transport Phenomena in Porous Media, III, Elsevier, John, Wiley & Sons Ltd., England, 2005, pp. 418–440.
[28] F.M. White, Fluid Mechanics, 5th ed., McGraw-Hill, New York, 2003.
[29] F.D. Incropera, D.P. DeWitt, Fundamentals of Heat and Mass Transfer, John Wiley & Sons, New York, 1995.
[30] C.L. Yaws, Handbook of Transport Property Data: Viscosity, Thermal Conductivity and Diffusion Coefficients of Liquids and Gases, Gulf Pub. Co., Houston, TX, 1995.
[31] W. Liu, C.Y. Wang, Three-dimensional, two-phase modeling of direct methanol fuel cells, in: 209th ECS Meeting, Denver, Colorado, 2006 (Abstract # 1141).
[32] G.Q. Lu, P.C. Lim, F.Q. Liu, C.Y. Wang, Int. J. Energy Res. 29 (2005) 1041–1050.
[33] X. Ren, T.E. Springer, S. Gottesfeld, J. Electrochem. Soc. 147 (2000) 92–98.
[34] E. Kjeang, J. Goldak, M.R. Golriz, J. Gub, D. James, K. Kordesch, J. Power Sources 153 (2006) 89–99.
[35] R.H. Perry, D.W. Green, J.O. Maloney, Perry's Chemical Engineers' Handbook, McGraw-Hill, New York, 1984.
[36] K. Scott, C. Jackson, P. Argyropoulos, J. Power Sources 161 (2006) 885–892.
[37] Q. Ye, T.S. Zhao, H. Yang, J. Prabhuram, Electrochem. Solid-State Lett. 8 (2005) A52–A54.